Electronic Supplementary Information (ESI) for

Enhanced condensation kinetics in aqueous microdroplets driven by coupled surface reactions and gas-phase partitioning

Meng Li,[1#] Shu Yang,[2#] Meenal Rathi,[3] Satish Kumar,[3] Cari S. Dutcher,[2,3]* and Vicki H. Grassian[1]*

[1]Department of Chemistry and Biochemistry, University of California San Diego, La Jolla, CA 92093, United States
[2]Department of Mechanical Engineering, University of Minnesota, Minneapolis, MN 55455, United States
[3]Department of Chemical Engineering and Materials Science, University of Minnesota, Minneapolis, MN 55455, United States
[#]These authors contributed equally.
*Corresponding Authors. Email: vhgrassian@ucsd.edu (V.G.H), cdutcher@umn.edu (C.S.D)

The ESI contains additional details about the kinetic model and the experimental protocol, eight figures, four tables and references.

Role of evaporation of pyruvic acid (PA) and partitioning of water

The key role of PA evaporation and water partitioning in the time evolution PA concentration (m_{PA}, in the unit of mol kg^{-1}) can be explained by the following equation (same as equation (4) in the main text)

$$m_{PA} = \frac{1}{\frac{1}{4.5}+\frac{\Delta N_{ZA} k_{ZA} m_W}{N_{PA,o}-\Delta N_{PA}}} \quad \text{(ESI-1)}$$

Where $N_{PA,o}$ is the initial moles of PA, ΔN_{PA} is the reduced moles of PA, ΔN_{ZA} is the generated moles of zymonic acid (ZA), k_{ZA} represents the change of one mole of ZA corresponds to a change of k_{ZA} moles of water, and m_W is the molar mass of water. The term $\Delta N_{ZA} k_{ZA} m_W$ is the increase in water mass due to the formation of ZA. PA evaporation increases ΔN_{PA} and water partitioning (absorbed by ZA) increases $\Delta N_{ZA} k_{ZA} m_W$. Therefore, both PA evaporation and water partitioning accelerate the reduction rate of m_{PA}.

Since ZA is less hygroscopic than PA, the reaction of PA results in a greater water loss than the water absorption caused by the formation of ZA. This leads to a lower water content in microdroplets, compared to bulk solutions with identical initial PA concentration but lacking water partitioning. Consequently, the equilibrium of the condensation reaction shifts towards the product side (Figure S5) during the reaction in microdroplets relative to the corresponding bulk solution, as water is eliminated in the reaction.

Influence of non-equilibrium water loss following the sample preparation on size and concentration changes

Non-equilibrium water loss following the sample preparation is not expected to be significant, as the concentration of the bulk solution was purposefully made the same as the corresponding equilibrium droplet concentration at a given relative humidity (RH). For example, for experiments at 95% RH, the PA bulk solution used to generation droplets had a concentration of 4.5 mol kg^{-1}, identical to the PA concentration in aqueous microdroplets in equilibrium with 95% RH within the environmental cell. This is confirmed by the stable concentration during the induction period at a given RH, since non-equilibrium water loss would change the PA concentration. For instance, if the initial droplet concentration is lower than the corresponding equilibrium concentration, the droplet would lose water, resulting in an increase in PA concentration, which is not the case in our study. The stable PA concentration in the induction period at each of the RH conditions demonstrates that the droplet had already reached equilibrium with the surrounding RH by the time the first spectrum was collected. Therefore, the influence of non-equilibrium water loss on droplet size and concentration changes is negligible.

Determination of diffusion coefficients.

The diffusivities of PA and ZA in aqueous microdroplets are estimated by the semiempirical relationship developed by Bidstrup and Geankoplis for aqueous diffusivities of carboxylic acid[1]

$$D = \frac{6.6\times10^{-8}(XM)^{1/2}T}{\eta V^{0.6}} \quad \text{(ESI-2)}$$

Here, D is the diffusivity (cm^2 s^{-1}) of solute, X is a constant of 2.6 for water, M is the molecular weight of solvent (18 g mol^{-1} for water), T is the absolute temperature (K), η is the viscosity (centipoises) of solution and is estimated using the Aerosol Inorganic−Organic

Mixtures Functional groups Activity Coefficients (AIOMFAC) model[2] (aiomfac.lab.mcgill.ca) and the experiment RH and temperature. η was assumed to be unchanged during the droplet reaction and is determined with a mole ratio of 1:1 for PA and ZA. V is molar volume of solute at normal boiling point ($cm^3\ g^{-1}\ mole^{-1}$) and is estimated by the method of LeBas.[3]

The diffusivities of PA in N_2 is determined by the equation developed by Fuller et al.[4] for binary gas-phase diffusion coefficients

$$D_{AB} = \frac{10^{-3}T^{1.75}\left(\frac{1}{M_A}+\frac{1}{M_B}\right)^{1/2}}{p\left[\left(\sum_A v_i\right)^{1/3}+\left(\sum_B v_i\right)^{1/3}\right]^2} \quad \text{(ESI-3)}$$

Here, A and B represent PA and N_2, respectively. D_{AB} is the binary diffusion coefficient ($cm^2\ s^{-1}$), T is the absolute temperature (K), M_A and M_B are the molecular weight ($g\ mol^{-1}$), p is the pressure (atm), $\sum_A v_i$ is the diffusion volumes to be summed over atoms of PA, and $\sum_B v_i$ is the diffusion volumes of N_2 (17.9). The diffusivity of PA and ZA in aqueous droplets as well as PA in N_2 in the gas phase under different temperatures and 95% RH are shown in Table S3. The diffusivities of PA and ZA in aqueous droplets at different RHs and 295 K are shown in Table S4.

Electronic Supplementary Figures

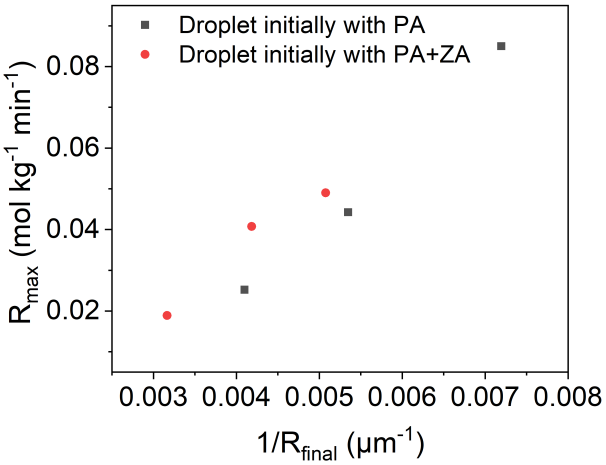

Figure S1. Comparison of the maximum apparent reaction rate (R_{max}) of PA versus the inverse of the final droplet size at the end of reaction ($1/R_{final}$) obtained from droplets initially containing only PA (black square) and droplets initially containing both PA and ZA (red circle). R_{max} was determined from the maximum slop of the PA concentration evolution curve in Figure 3a and 3b in the main text.

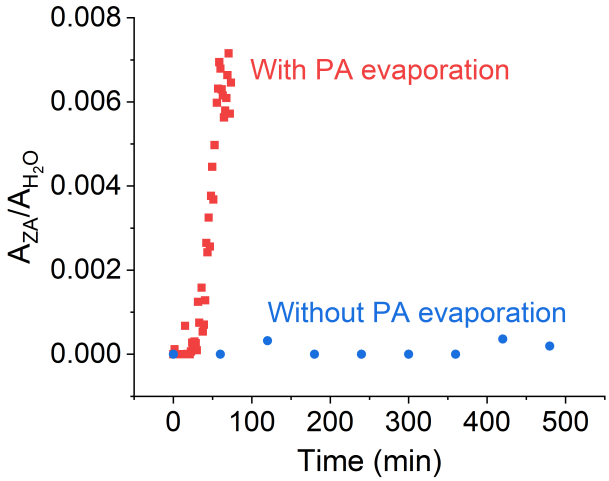

Figure S2. Comparison of the time evolution of the peak area ratio of ZA (at 796 cm^{-1}) and H_2O (from 3180 to 3750 cm^{-1}) (A_{ZA}/A_{H_2O}) in droplets with PA evaporation (red) and without PA evaporation (blue). The droplets correspond to those shown in Figure 4 in the main text, with the respective initial radius (R_o) of 211 μm and 207 μm under conditions with and without PA evaporation.

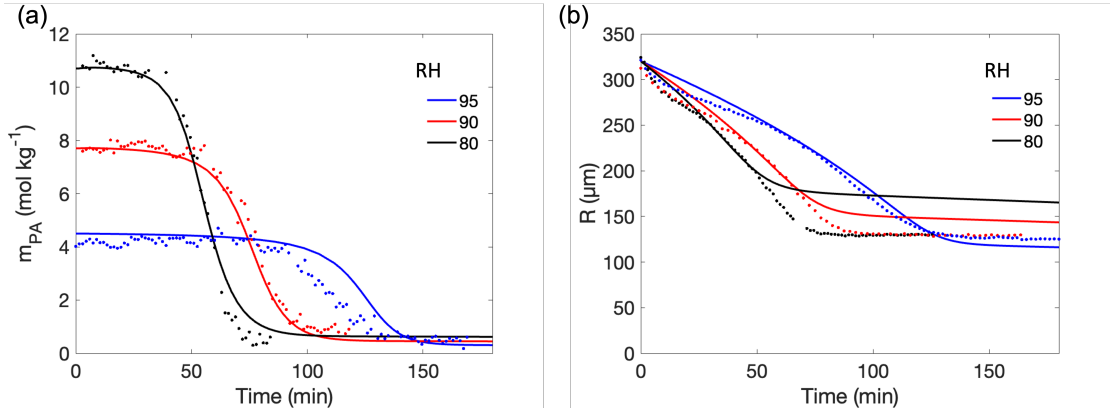

Figure S3. RH dependence of the autocatalytic PA condensation reaction. Time evolution of (a) PA concentration (m_{PA}) and (b) Droplet radius (R) in droplets with R_o of 320 ± 5 μm and at T=295 K. The dots present experimental data, and the lines are the modelling results. The reaction rate constants used here are the same as those in Figures 5d and 5f. The diffusivities of PA and ZA at various RHs are listed in Table S4.

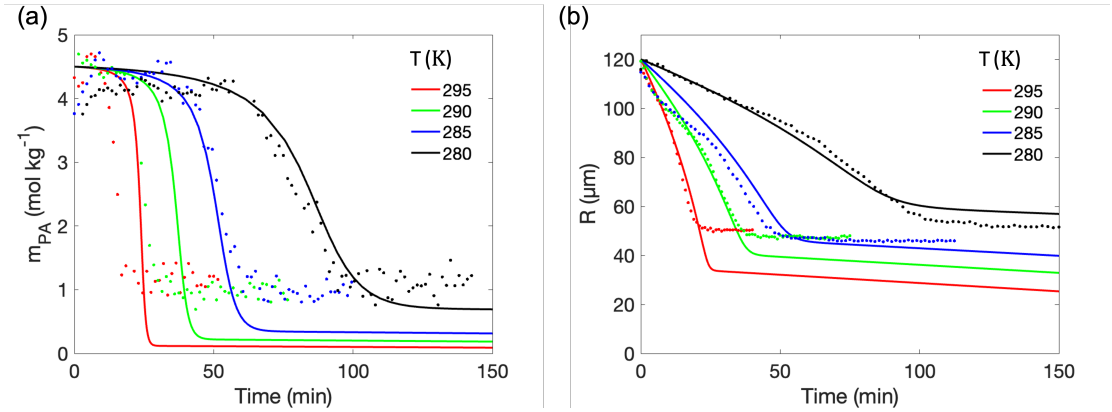

Figure S4. Temperature dependence of the autocatalytic PA condensation reaction. Time evolution of (a) m_{PA} and (b) R at various temperatures (T) with R_o=117 ± 5 μm and RH = 95%. The dots present experimental data, and the lines are the modelling results. The temperature-dependent reaction rate constants k_{fi} and evaporation rate constants k_{evp} are listed in Table S1. Here, the saturation pressure of PA at T is calculated by $P_{sat,PA} = \exp((276.11 - 70191.42/T - 55.8\ln(T/298.15)/R_g)$.[5] The diffusivities of PA and ZA at various T are listed in Table S3.

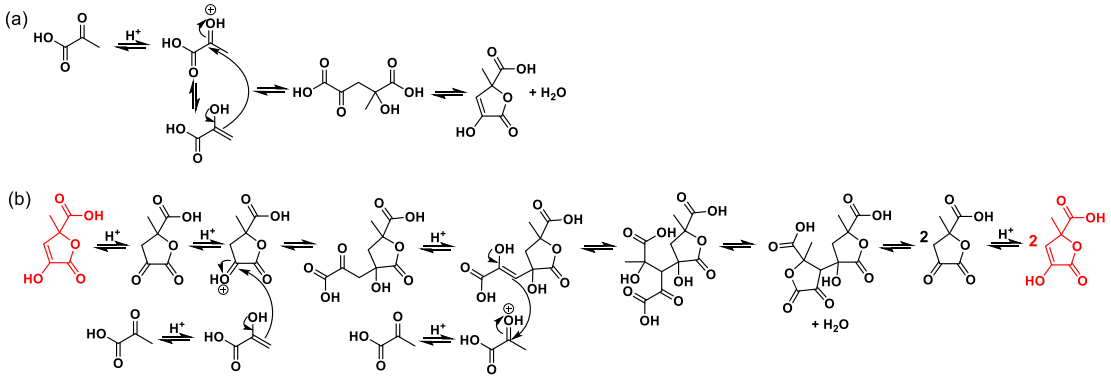

Figure S5: (a) Mechanism for the acid-catalyzed PA condensation reaction to form ZA.[6-9] (b) Proposed mechanism for the interfacial autocatalytic PA condensation reaction to form ZA in acidic aqueous microdroplets.

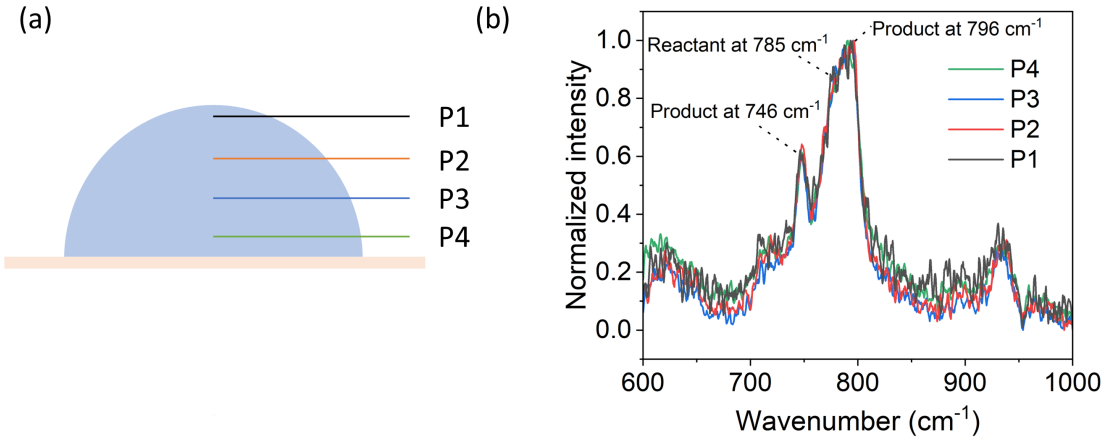

Figure S6. (a) Schematic illustrating the approximate sampling location. Note this is not drawn to scale. P1 to P4 may not be evenly spaced. (b) The normalized spectra obtained from different Z depth inside droplet with R_o = 444 μm (P4 to P1). These Raman spectra of the microdroplet were collected from the droplet center to near the surface during the formation of product. The time interval between two adjacent spectra was 1 minute. The nearly identical normalized spectra demonstrate that no significant concentration gradient of reactant and product can be detected under our experimental conditions (95% RH and 295 K), showing that the diffusion of product and reactant is faster compared to spectrum acquisition (1 min).

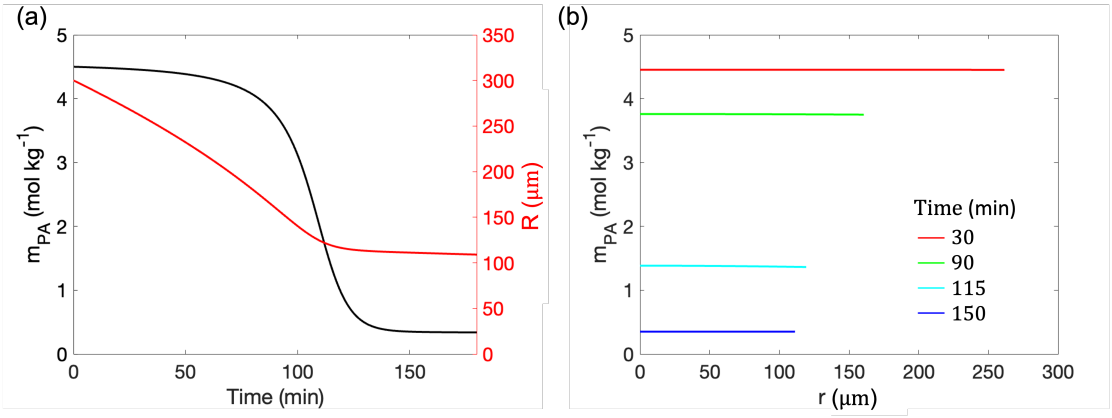

Figure S7. Kinetic modeling of autocatalytic condensation reaction of PA in aqueous microdroplets. (a) Time evolution of m_{PA} and R, and (b) m_{PA} versus radial positions (r) at four different times for a droplet with initial radii R_o=300 μm. The reaction rate constants used here are the same as those in Figures 5d and 5f.

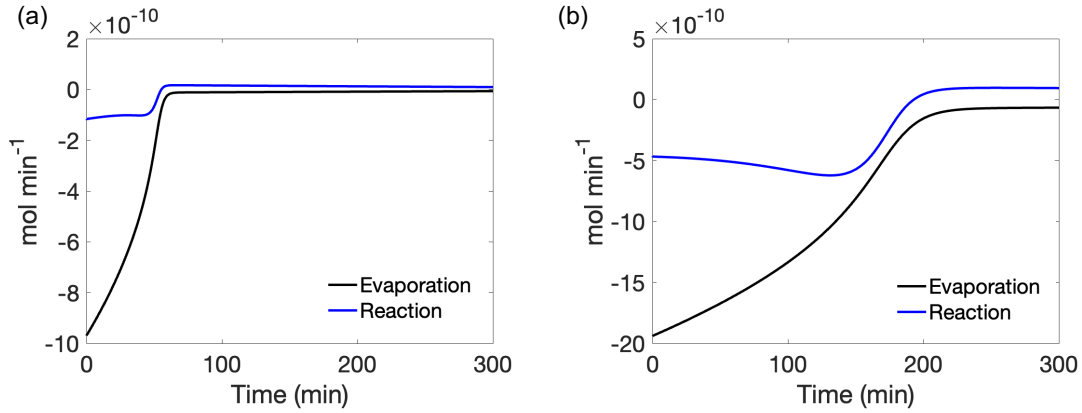

Figure S8. The number of moles of PA consumed through PA evaporation (black line) and through reactions (blue line) per minute for a droplet with R_o of 200 μm (a) and 400 μm (b). A negative value indicates that PA is consumed, while a positive value signifies that PA is generated (by backward reactions). In the equilibrium stage, the high m_{ZA} increases backward reaction rates, causing PA production to exceed its consumption. The produced PA matches the PA lost to evaporation, maintaining a constant m_{PA}. Note that the area enclosed by the lines over a given time period represents the total moles of PA consumed. The parameters used here are the same as those in Figures 6c-6d.

Electronic Supplementary Tables

Table S1. Reaction rate constants and evaporation rate constants at various temperatures used in Figure S4.

	k_{f1} (kg $mol^{-1}s^{-1}$)	k_{f2} (kg^2 $mol^{-2}s^{-1}$)	k_{evp}
295 K	0.25	0.65	0.6
290 K	0.23	0.62	0.45
285 K	0.2	0.58	0.45
280 K	0.18	0.54	0.3

Table S2. Molality of pure PA and pure ZA at different RHs.

	m_{PA} (mol kg^{-1})	m_{ZA} (mol kg^{-1})
95% RH	4.5	13.3
90% RH	7.7	18.7
85% RH	10.8	23.6

Table S3. Diffusivities of PA and ZA in aqueous droplets as well as PA in the gas phase (in N_2) at different temperatures and 95% RH.

	$\boldsymbol{D_{PA,l}}$ ($\mathbf{m^2\ s^{-1}}$)	$\boldsymbol{D_{ZA,l}}$ ($\mathbf{m^2\ s^{-1}}$)	$\boldsymbol{D_{PA,g}}$ ($\mathbf{m^2\ s^{-1}}$)
295 K	1.8×10^{-10}	1.3×10^{-10}	9.8×10^{-6}
290 K	1.3×10^{-10}	0.99×10^{-10}	9.5×10^{-6}
285 K	0.98×10^{-10}	0.71×10^{-10}	9.2×10^{-6}
280 K	0.68×10^{-10}	0.50×10^{-10}	9.0×10^{-6}

Table S4. Diffusivities of PA and ZA in aqueous droplets at different RHs and 295 K.

	$D_{PA,l}$ (m^2 s^{-1})	$D_{ZA,l}$ (m^2 s^{-1})
95% RH	1.8×10^{-10}	1.3×10^{-10}
90% RH	0.69×10^{-10}	0.5×10^{-10}
85% RH	0.33×10^{-10}	0.24×10^{-10}

References:

1. D. E. Bidstrup and C. J. Geankoplis, Aqueous molecular diffusivities of carboxylic acids, *J. Chem. Eng. Data*, 1963, **8**, 170-173.
2. A. Zuend, C. Marcolli, A. M. Booth, D. M. Lienhard, V. Soonsin, U. K. Krieger, D. O. Topping, G. McFiggans, T. Peter and J. H. Seinfeld, New and extended parameterization of the thermodynamic model AIOMFAC: calculation of activity coefficients for organic-inorganic mixtures containing carboxyl, hydroxyl, carbonyl, ether, ester, alkenyl, alkyl, and aromatic functional groups, *Atmos. Chem. Phys.*, 2011, **11**, 9155-9206.
3. G. L. Bas, *The molecular volumes of liquid chemical compounds*, Longmans, Green and Co., London, 1915.
4. E. N. Fuller, P. D. Schettler and J. C. Giddings, New method for prediction of binary gas-phase diffusion coefficients, *Ind. Eng. Chem.*, 1966, **58**, 18-27.
5. M. Frenkel, G. J. Kabo, K. N. Marsh, G. N. Roganov and R. C. Wilhoit, *Thermodynamics of organic compounds in the gas state*, CRC press, 1994.
6. R. J. Perkins, R. K. Shoemaker, B. K. Carpenter and V. Vaida, Chemical equilibria and kinetics in aqueous solutions of zymonic acid, *J. Phys. Chem. A*, 2016, **120**, 10096-10107.
7. K. J. Kappes, A. M. Deal, M. F. Jespersen, S. L. Blair, J.-F. Doussin, M. Cazaunau, E. Pangui, B. N. Hopper, M. S. Johnson and V. Vaida, Chemistry and photochemistry of pyruvic acid at the air–water interface, *J. Phys. Chem. A*, 2021, **125**, 1036-1049.
8. A. E. Reed Harris, A. Pajunoja, M. Cazaunau, A. Gratien, E. Pangui, A. Monod, E. C. Griffith, A. Virtanen, J.-F. Doussin and V. Vaida, Multiphase photochemistry of pyruvic acid under atmospheric conditions, *J. Phys. Chem. A*, 2017, **121**, 3327-3339.
9. S. S. Petters, T. G. Hilditch, S. Tomaz, R. E. H. Miles, J. P. Reid and B. J. Turpin, Volatility change during droplet evaporation of pyruvic acid, *ACS Earth Space Chem.*, 2020, **4**, 741-749.